Repetitive Early ^{68}Ga-FAPI PET Acquisition Comparing ^{68}Ga-FAPI-02, ^{68}Ga-FAPI-46, and ^{68}Ga-FAPI-74: Methodologic and Diagnostic Implications for Malignant, Inflammatory/Reactive, and Degenerative Lesions

Frederik M. Glatting[1–3], Jorge Hoppner[1,4], Dawn P. Liew[1], Antonia van Genabith[1], Anna-Maria Spektor[1], Levin Steinbach[1], Alexander Hubert[1], Clemens Kratochwil[1], Frederik L. Giesel[1,5], Katharina Dendl[1], Hendrik Rathke[1,6], Hans-Ulrich Kauczor[4,7], Peter E. Huber[2,3], Uwe Haberkorn[1,7,8], and Manuel Röhrich[1,7]

[1]Department of Nuclear Medicine, University Hospital Heidelberg, Heidelberg, Germany; [2]Clinical Cooperation Unit Molecular and Radiation Oncology, German Cancer Research Center, Heidelberg, Germany; [3]Department of Radiation Oncology, University Hospital Heidelberg, Heidelberg, Germany; [4]Department of Diagnostic and Interventional Radiology, University of Heidelberg, Heidelberg, Germany; [5]Department of Nuclear Medicine, University Hospital Düsseldorf, Düsseldorf, Germany; [6]Department of Nuclear Medicine, Inselspital, Bern University Hospital, University of Bern, Bern, Switzerland; [7]Translational Lung Research Center Heidelberg, Member of the German Center for Lung Research DZL, Heidelberg, Germany; and [8]Clinical Cooperation Unit Nuclear Medicine, German Cancer Research Center, Heidelberg, Germany

^{68}Ga-labeled fibroblast activation protein (FAP) inhibitor (^{68}Ga-FAPI) PET targets ^{68}Ga-FAPI–positive activated fibroblasts and is a promising imaging technique for various types of cancer and nonmalignant pathologies. However, discrimination between malignant and nonmalignant ^{68}Ga-FAPI–positive lesions based on static PET with a single acquisition time point can be challenging. Additionally, the optimal imaging time point for ^{68}Ga-FAPI PET has not been identified yet, and different ^{68}Ga-FAPI tracer variants are currently used. In this retrospective analysis, we evaluate the diagnostic value of repetitive early ^{68}Ga-FAPI PET with ^{68}Ga-FAPI-02, ^{68}Ga-FAPI-46, and ^{68}Ga-FAPI-74 for malignant, inflammatory/reactive, and degenerative lesions and describe the implications for future ^{68}Ga-FAPI imaging protocols. **Methods:** Whole-body PET scans of 24 cancer patients were acquired at 10, 22, 34, 46, and 58 min after the administration of 150–250 MBq of ^{68}Ga-FAPI tracer molecules (8 patients each for ^{68}Ga-FAPI-02, ^{68}Ga-FAPI-46, and ^{68}Ga-FAPI-74). Detection rates and SUVs (SUV_{max} and SUV_{mean}) for healthy tissues, cancer manifestations, and nonmalignant lesions were measured, and target-to-background ratios (TBR) versus blood and fat were calculated for all acquisition time points. **Results:** For most healthy tissues except fat and spinal canal, biodistribution analysis showed decreasing uptake over time. We analyzed 134 malignant, inflammatory/reactive, and degenerative lesions. Detection rates were minimally reduced for the first 2 acquisition time points and remained at a constant high level from 34 to 58 min after injection. The uptake of all 3 variants was higher in malignant and inflammatory/reactive lesions than in degenerative lesions. ^{68}Ga-FAPI-46 showed the highest uptake and TBRs in all pathologies. For all variants, TBRs versus blood constantly increased over time for all pathologies, and TBRs versus fat were constant or decreased slightly. **Conclusion:** ^{68}Ga-FAPI PET/CT is a promising imaging modality for malignancies and benign lesions. Repetitive early PET acquisition added diagnostic value for the discrimination of malignant from nonmalignant ^{68}Ga-FAPI–positive lesions. High detection rates and TBRs over time confirmed that PET acquisition earlier than 60 min after injection delivers high-contrast images. Additionally, considering clinical feasibility, acquisition at 30–40 min after injection might be a reasonable compromise. Different ^{68}Ga-FAPI variants show significant differences in time-dependent biodistributional behavior and should be selected carefully depending on the clinical setting.

Key Words: fibroblast activation protein; FAPI; PET; cancer; biodistribution

J Nucl Med 2022; 63:1844–1851
DOI: 10.2967/jnumed.122.264069

PET using fibroblast activation protein (FAP) inhibitor labeled with ^{68}Ga (^{68}Ga-FAPI) targets ^{68}Ga-FAPI–positive fibroblasts that occur in the tumor microenvironment as cancer-associated fibroblasts (*1–3*), as well as in benign pathologies, such as fibrotic (*4,5*), reactive (*6*), and degenerative (*7*) processes. Numerous studies have demonstrated the great potential of ^{68}Ga-FAPI PET/CT for imaging of various malignant (*8,9*) and nonmalignant diseases, especially fibrotic and inflammatory (*10–13*) and degenerative (*14,15*) diseases.

In most of these studies, static PET images were acquired 1 h after injection of the ^{68}Ga-FAPI tracer, in analogy to ^{18}F-FDG PET. Some studies have evaluated ^{68}Ga-FAPI PET/CT at different acquisition time points or dynamic ^{68}Ga-FAPI PET (*13,16–19*), but the reported results are based on small numbers of patients and are partially conflicting. To date, it is not clear which time point should be considered optimal for ^{68}Ga-FAPI PET acquisition. Moreover, a large variety of ^{68}Ga-FAPI tracer variants is currently in use at different centers, and only a small number of preclinical (*20*) and clinical (*6,8,16*) studies have compared different ^{68}Ga-FAPI variants regarding their biodistribution and imaging properties for different pathologies.

In this retrospective analysis, we evaluated a repetitive early ^{68}Ga-FAPI PET protocol with PET acquisition at 10, 22, 34, 46, and 58 min after tracer application, wherein 3 ^{68}Ga-FAPI variants (^{68}Ga-FAPI-02, ^{68}Ga-FAPI-46, and ^{68}Ga-FAPI-74) were applied in 8 patients. The aim of this study was to describe the differential biodistribution and imaging

Received Feb. 25, 2022; revision accepted May 16, 2022.
For correspondence or reprints, contact Manuel Röhrich (manuel.roehrich@med.uni-heidelberg.de).
Published online May 26, 2022.

properties of the 3 variants over time for malignant, degenerative, and inflammatory/reactive lesions and to determine an optimal time point for ^{68}Ga-FAPI PET acquisition with respect to optimal imaging quality, detection rate, and workflow.

MATERIALS AND METHODS

Patient Characterization

Twenty-four patients (aged 34–83 y; average, 61 y) with different types of cancer were examined by ^{68}Ga-FAPI PET/CT. To avoid potential therapy effects on ^{68}Ga-FAPI PET signaling, only patients without surgery, radiotherapy, or chemotherapy within the last 4 wk were examined. Median intervals between treatments and ^{68}Ga-FAPI PET were 13 mo (range, 1–240 mo) for surgery, 29 mo (range, 2–260 mo) for radiotherapy, and 7 mo (range, 1–240 mo) for chemotherapy. All patients were referred by their treating physicians for ^{68}Ga-FAPI PET/CT because of clinical indications. All patients gave written informed consent to the scientific evaluation of their personal data. This study was approved by the local institutional review board (study S-115/2020). Patient characteristics and tracer variants for each patient are given in Supplemental Table 1 (supplemental materials are available at http://jnm.snmjournals.org).

Repetitive ^{68}Ga-FAPI PET/CT

Diagnostic imaging was performed under the conditions of the updated declaration of Helsinki, §37 (Unproven Interventions in Clinical Practice), and in accordance with the German Pharmaceuticals Law §13 (2b) for medical reasons. FAPI tracers (FAPI-02, FAPI-46, and FAPI-74; 8 patients each) were labeled with ^{68}Ga as previously described (*20*) and applied intravenously (80 nmol/GBq). Within the first 10 min after tracer injection, CT scans were performed with a Biograph mCT Flow PET/CT scanner (Siemens Medical Solutions) using the following parameters: slice thickness of 5 mm, increment of 3–4 mm, soft-tissue reconstruction kernel, and CARE Dose4D. PET scans were acquired exactly 10, 22, 34, 46, and 58 min after tracer administration (named as time points 1, 2, 3, 4, and 5) with a standardized field of view allowing whole-body scans within 12 min in 3 dimensions (matrix, 200 × 200) in FlowMotion at 1.6 cm/min. Emission data were corrected for random events, scatter, and decay. Reconstruction used an ordered-subset expectation maximization algorithm with 2 iterations and 21 subsets, gauss-filtered to a transaxial resolution of 5 mm in full width at half maximum. Attenuation correction was performed using low-dose non-enhanced CT data.

Image Analysis and Quantification

Volumes of Interest (VOIs). SUVs using a VOI technique were quantitatively assessed by 2 of the authors independently at first, followed by a consensus reading between them. Tracer biodistribution in patients and uptake at pathologic sites were quantified by SUV_{mean} and SUV_{max}. Normal organs were evaluated using a sphere, placed inside the organ parenchyma, with a diameter of 5 mm for oral

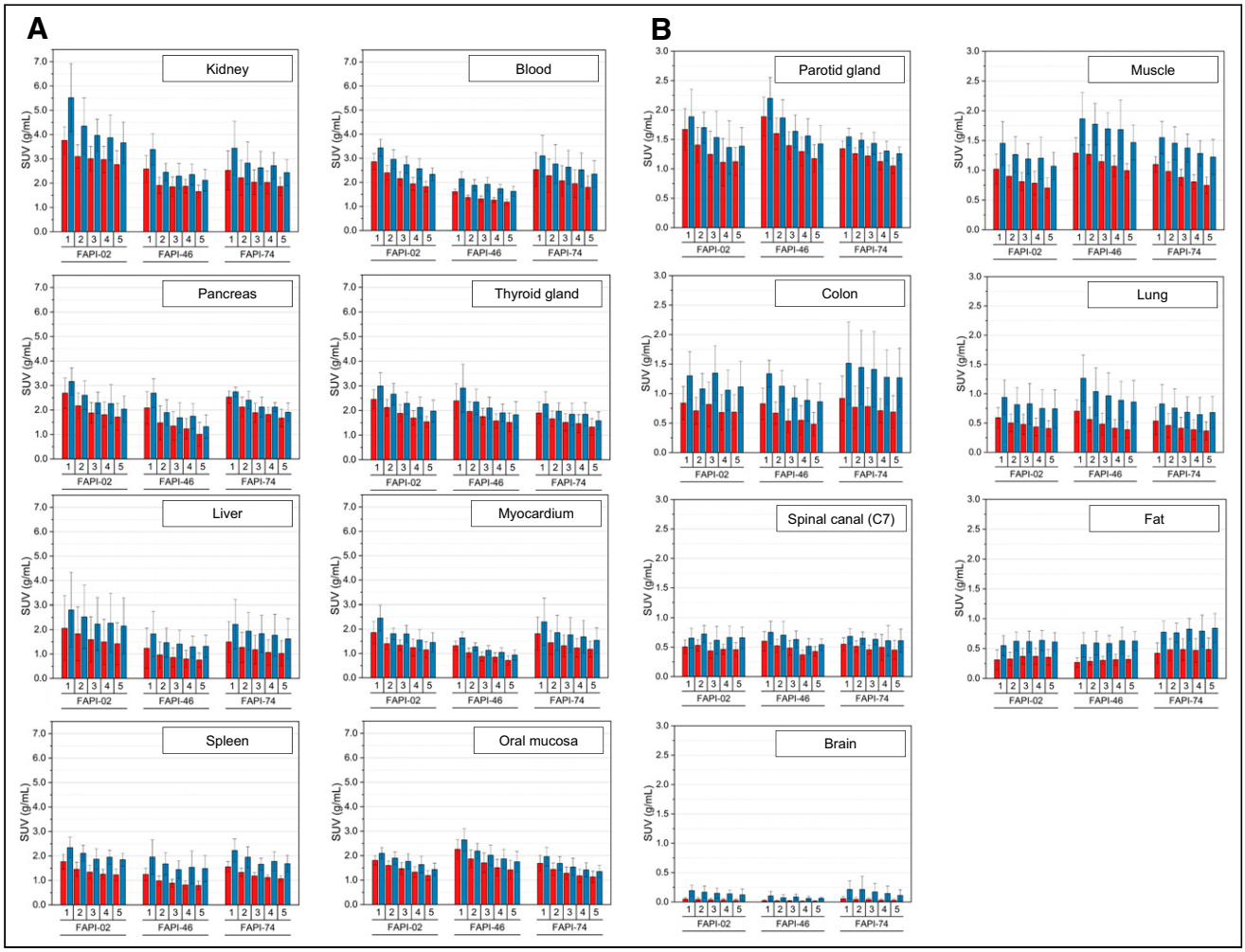

FIGURE 1. Biodistribution analysis (SUV_{mean} [red] and SUV_{max} [blue] ± SD) of 24 patients, 8 patients per ^{68}Ga-FAPI variant, with high-uptake (A) and low-uptake (B) tissues over time at acquisition time points of 10 min (1), 22 min (2), 34 min (3), 46 min (4), and 58 min (5) after application of ^{68}Ga-FAPI variants of ^{68}Ga-FAPI-02, ^{68}Ga-FAPI-46, or ^{68}Ga-FAPI-74.

mucosa, parotid glands, thyroid, myocardium, pancreas, kidneys, and spinal canal (C7); 10 mm for blood, colon, and fat tissue; and 15 mm for brain, lungs, liver, spleen, and muscles. VOIs for blood were drawn at the beginning of the descending aorta on the first axial slide on which the aortic arch was no longer visible, and VOIs for fat were drawn within gluteal fat tissue at the height of the acetabulum. Respecting SUV calculation for pathologies, spheric regions of interest were drawn around the lesions on ^{68}Ga-FAPI PET images acquired at 58 min after injection and were automatically adapted to a 3-dimensional volume by PMOD software (PMOD Technologies LLC) at a 50%–70% isocontour. All VOIs for normal tissues and pathologies were automatically transferred to the previous time points by PMOD software in order to achieve identical intraindividual VOIs.

We determined dominating tracer variants for each tissue by evaluating the mean absolute SUV_{max} and SUV_{mean} at the initial and following time points. Variants with the highest values and marked differences from the other 2 variants were considered dominant. If the differences between different ^{68}Ga-FAPI tracers were not distinct, they were considered approximately equal.

Lesions were classified as malignant, inflammatory/reactive, or degenerative on the basis of clinical information and CT morphology. Only lesions with highly suggestive characteristics for 1 of these classes were analyzed. Detection rates for all classes of lesions were determined by 3 of the authors as previously described (*18*).

An increase, constant level, or decrease in ^{68}Ga-FAPI uptake was determined on the basis of visual assessment and the trends in mean absolute SUV_{max} or SUV_{mean} over time.

Statistical Analysis

We performed descriptive analyses for patients and their characteristics. For determination of SUVs, median and range were used. The correlation of ^{68}Ga-FAPI uptake within or outside the lesions was determined using a 2-sided *t* test. A *P* value of less than 0.05 was defined as statistically significant. Excel (version 2111; Microsoft) and Origin (version 2021b; OriginLab Corp.) were used for statistical analyses.

RESULTS

Patient Cohort

Supplemental Table 1 summarizes the demographic and clinical data of all patients. Overall, 1 patient was treatment-naïve, having metastasis at the initial presentation. Of the 23 patients with suspected recurrence or progression after resection, chemotherapy, or radiotherapy, some patients showed evidence of a local tumor only (6 patients), metastasis only (8 patients), both local tumor and metastasis (6 patients), or no tumor (3 patients).

Biodistribution

Figure 1 shows the biodistribution in terms of SUV_{max} and SUV_{mean} over time for all physiologic tissues. Organs were categorized as having high or low ^{68}Ga-FAPI avidity (B). For most tissues, SUV_{max} and SUV_{mean} decreased continuously, whereas SUV_{max} and SUV_{mean} tended to increase for fat tissue and to remain constant for the spinal canal. By comparing tissue uptake for the 3 variants, Figure 2 shows the dominating variant for each tissue.

For each variant, Figure 3 shows representative maximum-intensity projections and axial ^{68}Ga-FAPI PET/CT images of blood pool, lungs, and muscles. In accordance with the data of Figure 2, these typical examples underline the biodistribution of the variants and show that the highest uptake by blood was for ^{68}Ga-FAPI-02. However, the highest uptake by muscle tissue was for ^{68}Ga-FAPI-46, according to the kinetics shown in Figure 1 and the data of Figure 2.

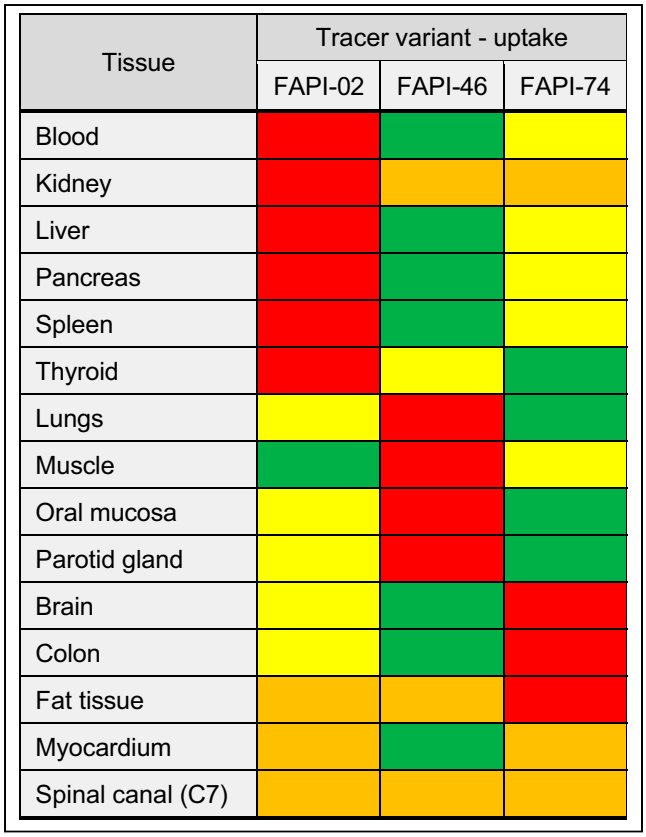

FIGURE 2. Dominating ^{68}Ga-FAPI variant for each considered tissue, with red indicating highest uptake; yellow, medium uptake; green, lowest uptake; and orange, approximately equal uptake.

Supplemental Figure 1 shows an intertissue comparison of the biodistribution at 34 and 58 min after injection.

Detection Rate

On the basis of clinical information and CT morphology, 134 lesions were classified as malignant, inflammatory/reactive, or degenerative and were used for further analysis. Three lesions were labeled "other" because they could not be matched with 1 of the 3 classes and were not further analyzed. Table 1 summarizes all 137 lesions. Lesions rated as malignant numbered 34 of 49 (69.4%) for ^{68}Ga-FAPI-02, 21 of 52 (40.4%) for ^{68}Ga-FAPI-46, and 16 of 36 (44.4%) for ^{68}Ga-FAPI-74.

Respecting ^{68}Ga-FAPI-02 and ^{68}Ga-FAPI-74, 2 malignant lesions of 47 total lesions (4.3%) and 1 malignant lesion of 36 total lesions (2.8%), respectively, could not be detected on imaging at the first time point but were detectable at the following 4 time points. For ^{68}Ga-FAPI-46, a retroperitoneal liposarcoma remained undetected over all 5 time points. Two degenerative lesions of 52 total lesions (3.8%) were not detected at the first time point, and 1 of these (1.9%) was not seen at the second time point either. Both were detectable at the following time points. All inflammatory/reactive lesions were detected at all 5 time points for each variant (Table 2).

Uptake over Time in Malignant, Inflammatory/Reactive, and Degenerative Lesions

The different types of lesions differed in their time-dependent uptake. Figure 4 provides an overview of the SUV_{max} and SUV_{mean}

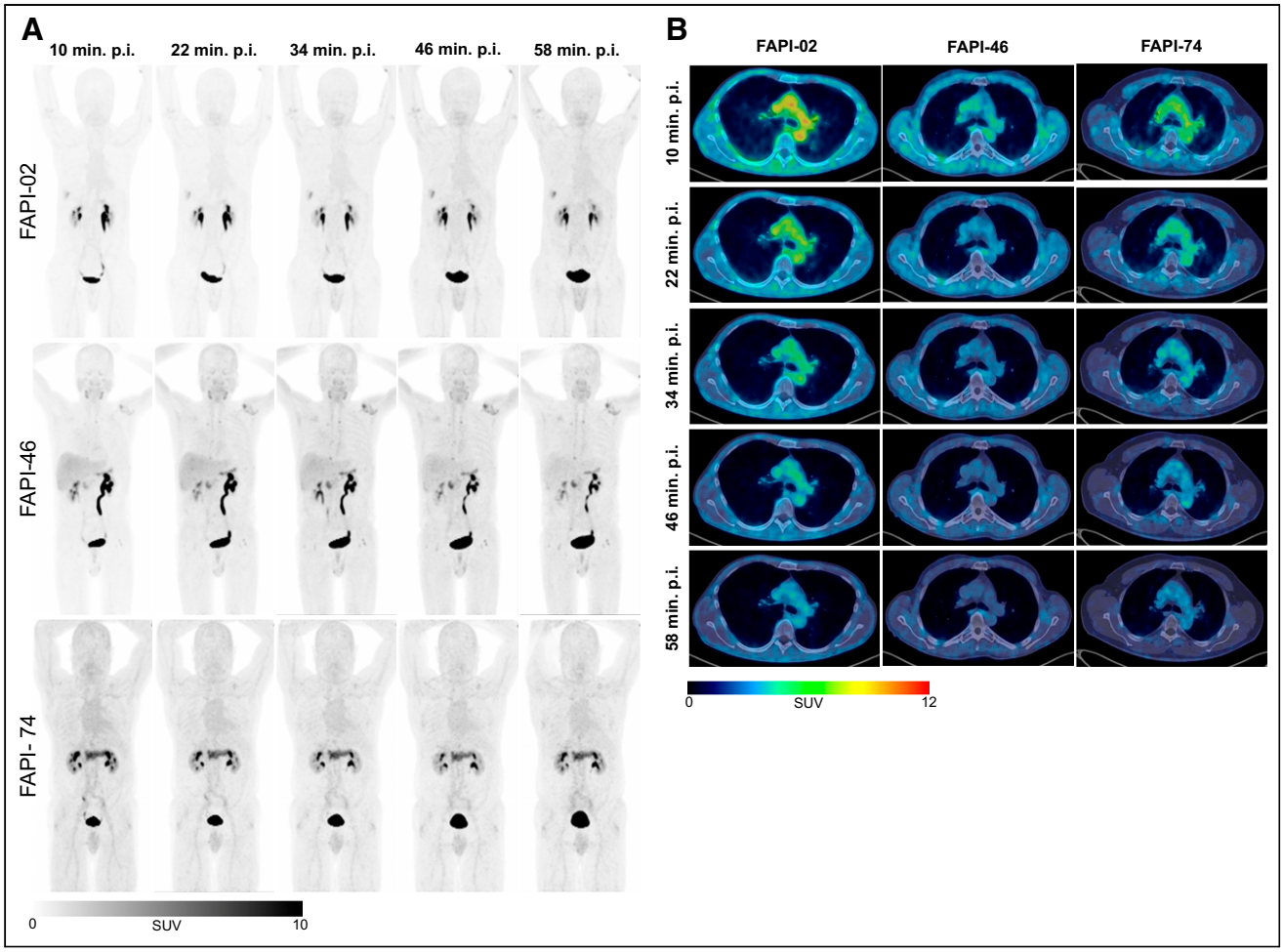

FIGURE 3. (A) Representative maximum-injection projections of ^{68}Ga-FAPI PET/CT for ^{68}Ga-FAPI-02 (top row, 56-y-old man with resected pancreatic carcinoma, staging for metastases, no local recurrence, single hepatic metastasis), ^{68}Ga-FAPI-46 (middle row, 64-y-old man with pancreatic cancer, staging for suspected local recurrence, no metastases), and ^{68}Ga-FAPI-74 (bottom row, 60-y-old man with pancreatic carcinoma, staging in advance of radiation therapy, primary, single hepatic metastasis) over time with acquisition time points of 10 min (1), 22 min (2), 34 min (3), 46 min (4), and 58 min (5) after application. (B) Representative axial ^{68}Ga-FAPI PET/CT images of upper thorax showing uptake for blood, muscle, and lungs over time with acquisition time points of 10 min (1), 22 min (2), 34 min (3), 46 min (4), and 58 min (5) after application of ^{68}Ga-FAPI-02 (left column, 56-y-old man with resected pancreatic carcinoma, staging for metastases, no local recurrence, single hepatic metastasis), ^{68}Ga-FAPI-46 (middle column, 58-y-old man with retroperitoneal liposarcoma, staging in advance of neoadjuvant radiation therapy, primary, 3 metastases), and ^{68}Ga-FAPI-74 (60-y-old man with pancreatic carcinoma, staging in advance of radiation therapy, primary, single hepatic metastasis). p.i. = after injection.

kinetics of different types of lesions at the 5 acquisition times, allowing a comparison between variants. Respecting ^{68}Ga-FAPI-02, malignant lesions showed a slightly increasing uptake over time whereas benign lesion tended to be constant or slightly decreasing. The absolute values among the 3 lesion types were similar.

For ^{68}Ga-FAPI-46, malignant and inflammatory/reactive lesions show higher uptake than degenerative lesions. Moreover, the uptake within these lesions was higher than for ^{68}Ga-FAPI-02 or ^{68}Ga-FAPI-74. Additionally, regarding ^{68}Ga-FAPI-46, malignant and inflammatory/reactive lesions featured a slope over time, whereas uptake by degenerative lesions remained roughly unchanged.

^{68}Ga-FAPI-74 showed higher uptake in malignant and inflammatory/reactive lesions than in degenerative lesions. The uptake remained constant or increased only slowly for malignant and inflammatory/reactive lesions over time. However, the degenerative pathologies showed an increasing uptake over time, finally approaching the level of the 2 other types of pathologies. This finding is demonstrated in Figure 5 by a ^{68}Ga-FAPI-74 PET/CT scan of a patient with a solitary hepatic metastasis, pancreatitis, and an insertion-related tendinopathy in the right trochanter region. The uptake associated with the insertion-related tendinopathy increased over time, whereas the uptake by the hepatic metastasis and pancreatitis decreased slightly (Supplemental Table 2).

Target-to-Background Ratios (TBRs) over Time in Malignant, Inflammatory/Reactive, and Degenerative Lesions

Because fat tissue showed an increasing ^{68}Ga-FAPI uptake for all 3 variants over time, contrary to the other healthy tissues, and because uptake by fat can easily be measured in a clinical setting, the SUV_{max} and SUV_{mean} of fat tissue were used to calculate TBRs versus fat tissue in addition to TBRs versus blood. The corresponding graphs are in Figure 6.

In comparison with ^{68}Ga-FAPI-02 and ^{68}Ga-FAPI-74, ^{68}Ga-FAPI-46 showed a higher TBR versus blood and versus fat for

TABLE 1
Number of Malignant, Inflammatory/Reactive, and Degenerative Pathologies for Each Radiotracer

Variant	Pathology	*n*
^{68}Ga-FAPI-02	Total	49 (100.0%)
	Malignant	34 (69.4%)
	Inflammatory/reactive	4 (8.2%)
	Degenerative	9 (18.4%)
	Other	2 (4.1%)
^{68}Ga-FAPI-46	Total	52 (100.0%)
	Malignant	21 (40.4%)
	Inflammatory/reactive	8 (15.4%)
	Degenerative	22 (42.3%)
	Other	1 (1.9%)
^{68}Ga-FAPI-74	Total	36 (100.0%)
	Malignant	16 (44.4%)
	Inflammatory/reactive	9 (25.0%)
	Degenerative	11 (30.6%)
	Other	0 (0.0%)

malignant, inflammatory/reactive, and degenerative lesions at all acquisition times. In contrast to the curve progression of TBR versus blood, which increased over time for all variants at different slopes for all 3 kinds of lesions, TBR versus fat tended to remain constant or to decrease slightly. This behavior was particularly evident for ^{68}Ga-FAPI-02 in inflammatory/reactive pathologies, whereas ^{68}Ga-FAPI-74 still showed an increase in TBR versus fat over time only for degenerative lesions.

DISCUSSION

In this retrospective analysis, we found different time-dependent biodistributions for the 3 variants ^{68}Ga-FAPI-02, ^{68}Ga-FAPI-46, and ^{68}Ga-FAPI-74, implicating the benefit of careful selection of the variant depending on the tissue of interest and the clinical setting. Furthermore, this study demonstrated the differential behavior of malignant, inflammatory/reactive, and degenerative lesions over time by considering the uptake and TBR versus blood and fat tissue.

Time-Dependent Biodistribution of ^{68}Ga-FAPI Variants

Biodistribution analysis showed that SUV_{max} and SUV_{mean} declined over time for all tissues except fat tissue (increase) and spinal cord (constant). The detection rate for each variant was slightly reduced at 10 min after injection for all variants; for ^{68}Ga-FAPI-46, the detection rate was still reduced at 22 min but was stable at a high level between 34 and 58 min. To optimize the selection of ^{68}Ga-FAPI variants, we identified the dominating variant for each tissue. The variant showing the lowest uptake, and thus lowest background, within healthy tissue is considered a potential optimal variant. Given the differential muscle-to-fat ratio between female and male patients and the variability in body mass, it might be of interest to analyze fat and muscle signaling with respect to the sexes and body mass index in order to minimize background activity through optimal variant selection. This analysis may also be interesting with respect to reduction of radiation exposure but would require a larger cohort than ours. However, as the magnitude of uptake by malignant and benign lesions, and thereby the TBRs, also affects the suitability of a variant for a certain clinical context, uptake and TBR over time were analyzed in malignant, inflammatory/reactive, and degenerative lesions. Generally, the uptake was higher in malignant and inflammatory/reactive lesions than in degenerative lesions for all 3 variants. However, different trends could be observed for the different variants. The slightly increasing or constant uptake of ^{68}Ga-FAPI-02 over

TABLE 2
Detection Rates and Undetected Lesions at Different Acquisition Time Points

	Detection rate and undetected lesions				
Variant	10 min	22 min	34 min	46 min	58 min
^{68}Ga-FAPI-02	95.7	100,0	100,0	100.0	100.0
Malignant	2/34	0/31*	0/34	0/34	0/34
Inflammatory/reactive	0/4	0/4	0/4	0/9	0/4
Degenerative	0/9	0/6*	0/9	0/9	0/9
^{68}Ga-FAPI-46	94.1	96.1	98.0	98.0	98.0
Malignant	1/21	1/21	1/21	1/21	1/21
Inflammatory/reactive	0/8	0/8	0/8	0/8	0/8
Degenerative	2/22	1/22	0/22	0/22	0/22
^{68}Ga-FAPI-74	97.2	100.0	100.0	100.0	100.0
Malignant	1/1	0/16	0/16	0/16	0/16
Inflammatory/reactive	0/9	0/9	0/9	0/9	0/9
Degenerative	0/11	0/11	0/11	0/11	0/11

*In 1 patient with 3 malignant and 3 degenerative lesions, image acquisition failed at time point 2.
Data are percentages.

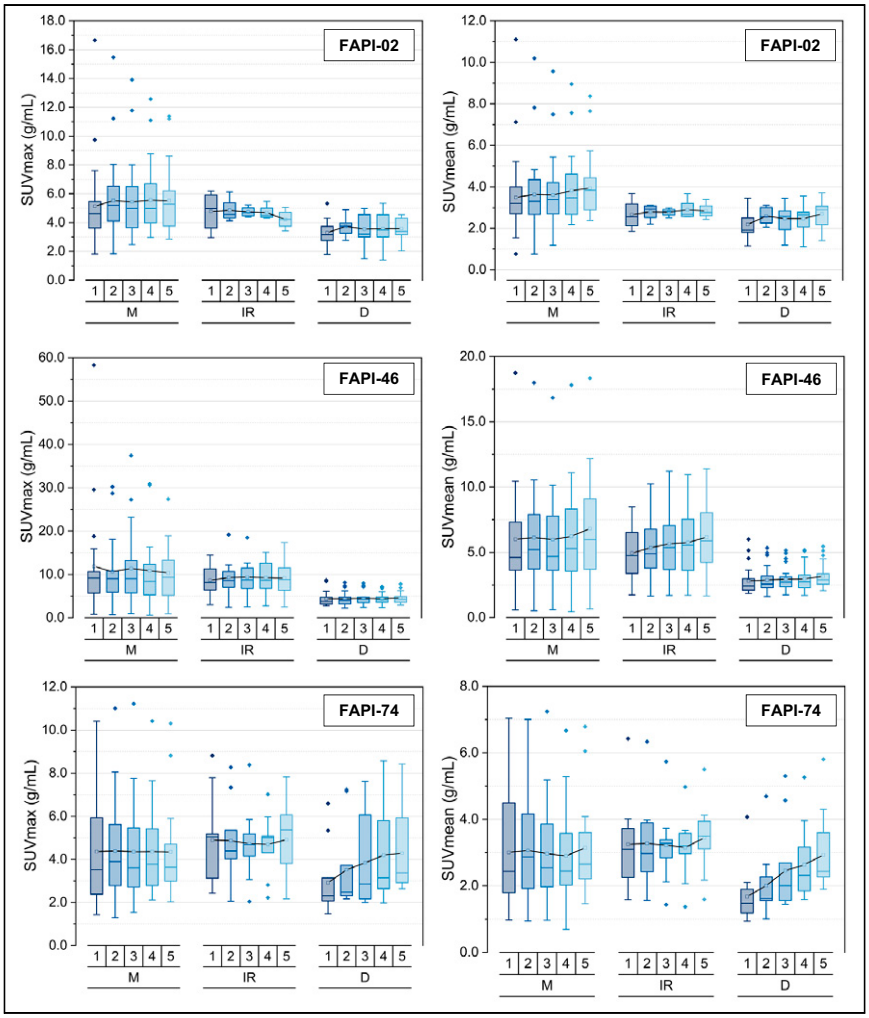

FIGURE 4. SUV_{max} and SUV_{mean} for malignant (M), inflammatory/reactive (IR), or degenerative (D) pathologies over time at 10 min (1), 22 min (2), 34 min (3), 46 min (4), and 58 min (5) after injection of 3 ^{68}Ga-FAPI variants (^{68}Ga-FAPI-02, ^{68}Ga-FAPI-46, and ^{68}Ga-FAPI-74). Boxes represent interquartile range, whiskers represent interquartile range of 1.5, horizontal line within box indicates median, and small box indicates mean. Data outliers are shown separately within graph. Trending lines regarding mean are shown.

time might indicate rapid uptake within the lesions and only a slow washout. Notably, in pathologies, ^{68}Ga-FAPI-46 showed the highest uptake of all variants. Along with the observation that ^{68}Ga-FAPI-46 showed a lower background activity in blood and other tissues, this variant also manifested the highest TBRs. Although ^{68}Ga-FAPI-46 featured a slightly increasing uptake within malignant and inflammatory/reactive lesions, there was an approximately constant uptake for degenerative lesions over time. ^{68}Ga-FAPI-74 showed an approximately constant level of uptake over time for malignant and inflammatory/reactive lesions but an increase for degenerative lesions.

Uptake and TBRs in Pathologies over Time

Most previous studies analyzing several acquisition time points demonstrated that time-dependent differences are small from 10 to 180 min after injection (*6,13,18,21*). Hu et al. observed a nonsignificant increase in SUV_{max} over time between 10 and 60 min after injection but calculated a significant increase in TBRs versus blood over time (*16*). In our study, we found only small differences in uptake among the 5 acquisition time points from 10 to 58 min after injection. Nevertheless, some trends could be concluded from the time-dependent uptake curves. First, uptake was higher in malignant and inflammatory/reactive lesions than in degenerative lesions for all 3 variants. Additionally, the malignant, inflammatory/reactive, and degenerative pathologies were distinguishable from one another by their absolute values and by their uptake progression over time. TBRs versus blood for all pathologies constantly increased over time for all variants, but at different slopes. In addition to the data presented here, we are planning to perform a separate analysis of this dataset focused on different subclasses of malignant, inflammatory/reactive, and degenerative lesions to identify further subgroups with differential uptake behaviors over time.

Diagnostic Value of Repetitive ^{68}Ga-FAPI Imaging and Implications for ^{68}Ga-FAPI PET Acquisition

^{68}Ga-FAPI PET/CT is a promising imaging modality for the detection of both malignant and benign pathologies. Nevertheless, the optimal acquisition time has not been clearly determined yet. The current level of knowledge is ambiguous and inconsistent. On the one hand, a recent study on ^{18}F-FAPI-42-PET/CT in 22 patients concluded that the optimal acquisition time was 60 min after injection, arguing that TBR versus blood was small initially and increased over time and that some lesions were undetected early after tracer application because of the small initial TBR versus blood (*16*). At the same time, the authors postulated that it might not be necessary to postpone the acquisition because tumor detection was not improved at later time points. On the other hand, Ferdinandus et al. reasoned—on the basis of a retrospective study including 69 patients who underwent ^{68}Ga-FAPI-46 PET 10 and 60 min after injection—that detection rates at the 2 acquisition times did not differ (*18*). Because of the improved feasibility and scan volume, the authors decided to implement early acquisition time points in future PET protocols.

Contrary to this conclusion and partly agreeing with the results of Hu et al., our study showed that the detection rate was slightly reduced at 10 min after injection (mainly caused by undetected malignant and degenerative lesions), thus arguing against performing clinical interpretation based on an early acquisition at 10 min after injection only. Along with the increasing TBR versus blood and the constant TBR versus fat over time, our finding suggested that the later time points would favor optimal clinical interpretations of PET/CT. Taking clinical practicability and feasibility into account along with a sufficient detection rate, acquisition at 30–40 min after injection is what we recommend and appears to be a reasonable compromise.

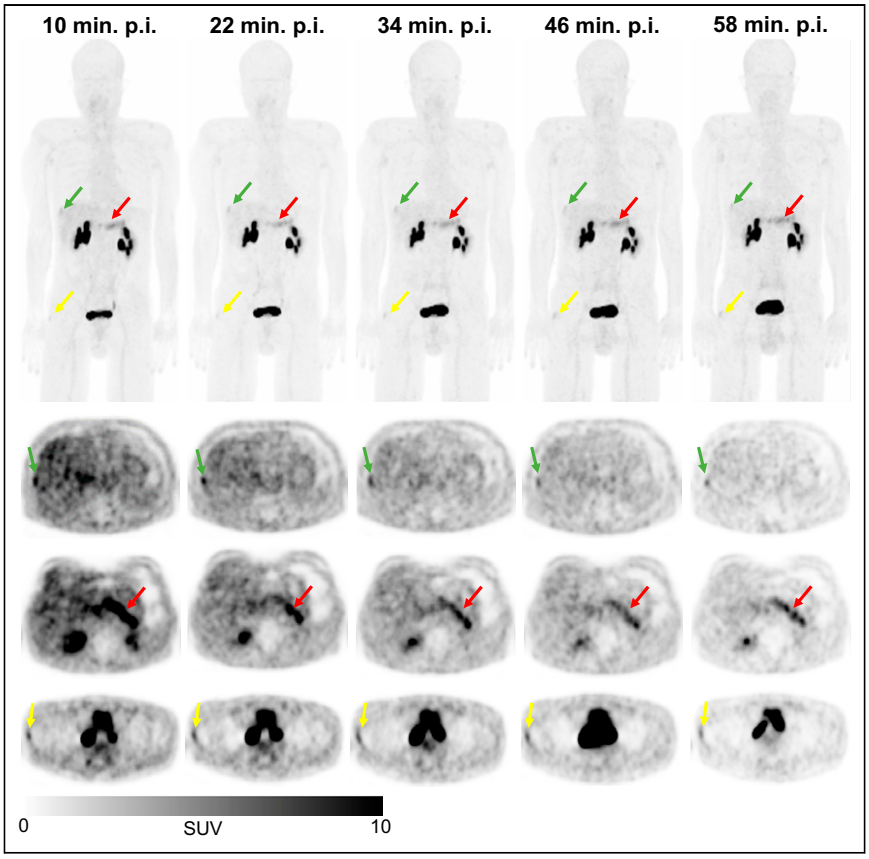

FIGURE 5. Example maximum-intensity projection (top) and axial PET/CT images of ^{68}Ga-FAPI-74 PET/CT scans (bottom) of 56-y-old man with pancreatic carcinoma after resection (no local recurrence, 4 metastases) over time with acquisition time points of 10 min (1), 22 min (2), 34 min (3), 46 min (4), and 58 min (5) after application. Clinically, patient showed hepatic metastasis (green arrows, second row, malignant manifestation), pancreatitis-related uptake (red arrows, third row, inflammatory lesion), and insertion-related tendinopathy in right trochanter region (yellow arrows, fourth row, degenerative lesion). p.i. = after injection.

Limitations

Several limitations of our analysis must be considered. One arises from the relatively low number (24) of patients included. Thus, conclusions on our data should be drawn with caution. A second limitation is that the lesions were not histologically confirmed. Our classification of pathologies had to be based on morphologic CT anomalies. Third, VOIs for the biodistribution analysis and for pathologies were defined using the dataset of the last acquisition time point and subsequently transferred to the previous time points in order to achieve identical intraindividual VOIs. This method can lead to uncertainty caused by movement artifacts within the first 4 acquisition time points, even though datapoints with visually obvious spatial differences were excluded from the dataset. Furthermore, because of the only small number of degenerative lesions examined using ^{68}Ga-FAPI-74, the surprising finding of markedly increasing uptake over time for degenerative lesions has to be interpreted carefully. Another limitation is the heterogeneity of the patient cohorts per variant. Although emphasis was put on pancreatic carcinoma within the patient groups, rarer malignancies such as liposarcomas, which are known to show FAP expression not only by cancer-associated fibroblasts but also by neoplastic cells, (*22*) were included and may have reduced the intergroup comparability. Since the results among tumor entities did not differ markedly, our conclusions might be relevant beyond the considered tumor entities.

CONCLUSION

^{68}Ga-FAPI PET/CT is a promising, innovative imaging modality for various malignancies and for various benign conditions. Repetitive early PET acquisition added diagnostic value for discrimination of malignant from nonmalignant ^{68}Ga-FAPI–positive lesions. TBRs and high detection rates over time confirmed that PET acquisition earlier than 60 min after injection delivers high-contrast images. According to our findings, by taking clinical practicability and feasibility into consideration along with a sufficient detection rate, we recommend acquisition at 30–40 min after injection. Different ^{68}Ga-FAPI variants show significant differences in their time-dependent biodistributional behavior and should be selected carefully depending on the clinical setting.

DISCLOSURE

This work was funded by grant 13341 from the Federal Ministry of Education and Research. Uwe Haberkorn, Clemens Kratochwil, and Frederik Giesel have filed a patent application for quinoline-based FAP-targeting agents for imaging and therapy in nuclear medicine and have shares of a consultancy group for iTheranostics. No other potential conflict of interest relevant to this article was reported.

ACKNOWLEDGMENT

We thank Oda Landmann-Fothergill for her language corrections.

KEY POINTS

QUESTION: What is the rationale for selection of optimal tracer variants and acquisition times for ^{68}Ga-FAPI PET?

PERTINENT FINDINGS: The background activity of most tissues decreased over time, and the detection rates for pathologies were minimally reduced at early acquisition times. ^{68}Ga-FAPI-46 showed the highest uptake in all pathologies. For all variants and pathologies, TBRs versus blood increased over time and TBRs versus fat were constant or decreased slightly.

IMPLICATIONS FOR PATIENT CARE: ^{68}Ga-FAPI variants show significant differences in their time-dependent biodistributional behavior and should be selected carefully depending on the clinical setting.

REFERENCES

1. LeBleu VS, Kalluri R. A peek into cancer-associated fibroblasts: origins, functions and translational impact. *Dis Model Mech.* 2018;11:dmm029447.
2. Kalluri R. The biology and function of fibroblasts in cancer. *Nat Rev Cancer.* 2016;16:582–598.
3. Sahai E, Astsaturov I, Cukierman E, et al. A framework for advancing our understanding of cancer-associated fibroblasts. *Nat Rev Cancer.* 2020;20:174–186.

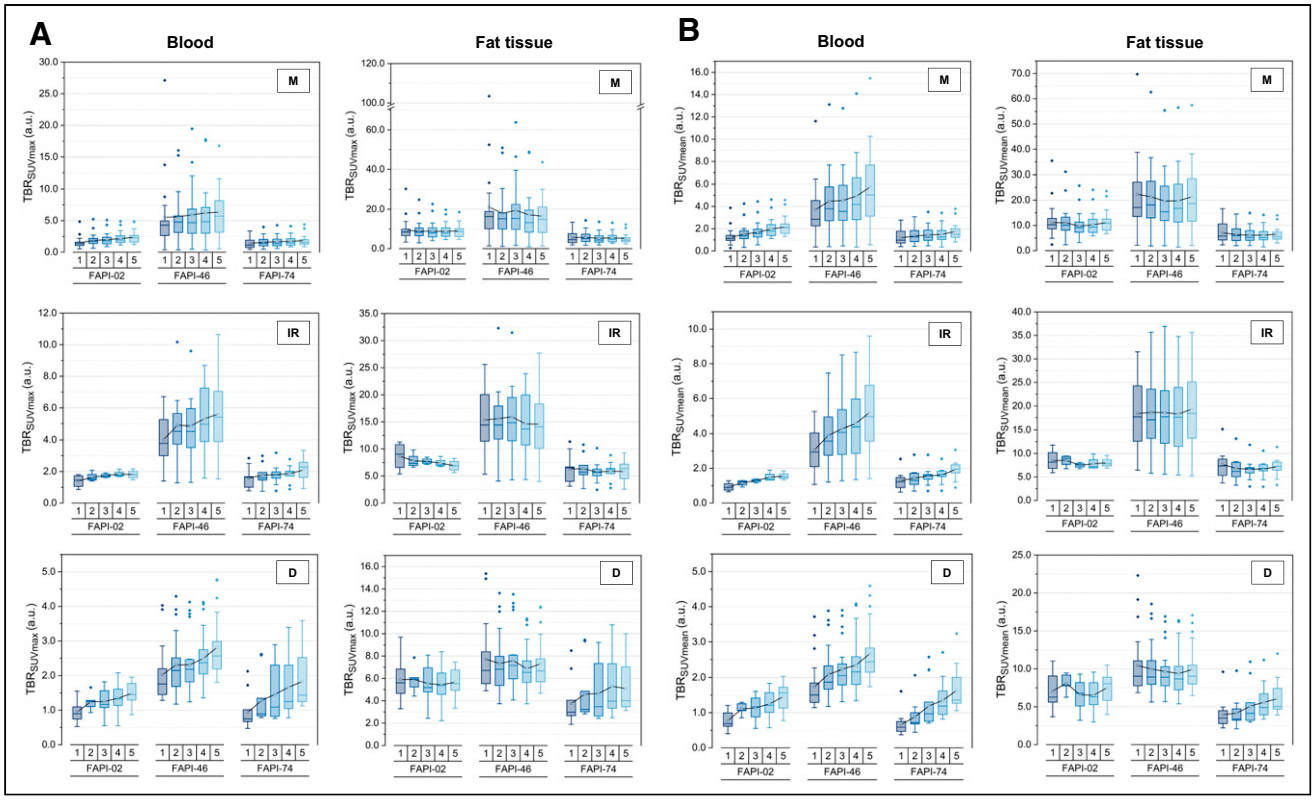

FIGURE 6. TBRs for SUV_{max} (A) and SUV_{mean} (B) regarding malignant (M), inflammatory/reactive (IR), and degenerative (D) pathologies vs. blood and vs. fat tissue for 3 ^{68}Ga-FAPI variants (^{68}Ga-FAPI-02, ^{68}Ga-FAPI-46, and ^{68}Ga-FAPI-74) over time, with acquisition time points of 10 min (1), 22 min (2), 34 min (3), 46 min (4), and 58 min (5) after injection. Boxes represent interquartile range, whiskers represent interquartile range of 1.5, horizontal line within box indicates median, and small box indicates mean. Data outliers are shown separately within graph. Trending lines regarding mean are shown. a.u. = arbitrary units.

4. Henderson NC, Rieder F, Wynn TA. Fibrosis: from mechanisms to medicines. *Nature.* 2020;587:555–566.
5. Affo S, Yu LX, Schwabe RF. The role of cancer-associated fibroblasts and fibrosis in liver cancer. *Annu Rev Pathol.* 2017;12:153–186.
6. Röhrich M, Naumann P, Giesel FL, et al. Impact of ^{68}Ga-FAPI PET/CT imaging on the therapeutic management of primary and recurrent pancreatic ductal adenocarcinomas. *J Nucl Med.* 2021;62:779–786.
7. Pap T, Dankbar B, Wehmeyer C, Korb-Pap A, Sherwood J. Synovial fibroblasts and articular tissue remodelling: role and mechanisms. *Semin Cell Dev Biol.* 2020; 101:140–145.
8. Kratochwil C, Flechsig P, Lindner T, et al. ^{68}Ga-FAPI PET/CT: tracer uptake in 28 different kinds of cancer. *J Nucl Med.* 2019;60:801–805.
9. Chen H, Pang Y, Wu J, et al. Comparison of [^{68}Ga]Ga-DOTA-FAPI-04 and [^{18}F] FDG PET/CT for the diagnosis of primary and metastatic lesions in patients with various types of cancer. *Eur J Nucl Med Mol Imaging.* 2020;47:1820–1832.
10. Luo Y, Pan Q, Yang H, Peng L, Zhang W, Li F. Fibroblast activation protein-targeted PET/CT with ^{68}Ga-FAPI for imaging IgG4-related disease: comparison to ^{18}F-FDG PET/CT. *J Nucl Med.* 2021;62:266–271.
11. Schmidkonz C, Rauber S, Atzinger A, et al. Disentangling inflammatory from fibrotic disease activity by fibroblast activation protein imaging. *Ann Rheum Dis.* 2020;79:1485–1491.
12. Zhou Y, Yang X, Liu H, et al. Value of [^{68}Ga]Ga-FAPI-04 imaging in the diagnosis of renal fibrosis. *Eur J Nucl Med Mol Imaging.* 2021;48:3493–3501.
13. Röhrich M, Leitz D, Glatting FM, et al. Fibroblast activation protein-specific PET/CT imaging in fibrotic interstitial lung diseases and lung cancer: a translational exploratory study. *J Nucl Med.* 2022;63:127–133.
14. Qin C, Song Y, Liu X, et al. Increased uptake of ^{68}Ga-DOTA-FAPI-04 in bones and joints: metastases and beyond. *Eur J Nucl Med Mol Imaging.* 2022;49: 709–720.
15. Liu H, Wang Y, Zhang W, Cai L, Chen Y. Elevated [^{68}Ga]Ga-DOTA-FAPI-04 activity in degenerative osteophyte in a patient with lung cancer. *Eur J Nucl Med Mol Imaging.* 2021;48:1671–1672.
16. Hu K, Wang L, Wu H, et al. [^{18}F]FAPI-42 PET imaging in cancer patients: optimal acquisition time, biodistribution, and comparison with [^{68}Ga]Ga-FAPI-04. *Eur J Nucl Med Mol Imaging.* 2022;49:2833–2843.
17. Wang S, Zhou X, Xu X, et al. Dynamic PET/CT Imaging of ^{68}Ga-FAPI-04 in Chinese subjects. *Front Oncol.* 2021;11:651005.
18. Ferdinandus J, Kessler L, Hirmas N, et al. Equivalent tumor detection for early and late FAPI-46 PET acquisition. *Eur J Nucl Med Mol Imaging.* 2021;48: 3221–3227.
19. Geist BK, Xing H, Wang J, et al. A methodological investigation of healthy tissue, hepatocellular carcinoma, and other lesions with dynamic ^{68}Ga-FAPI-04 PET/CT imaging. *EJNMMI Phys.* 2021;8:8.
20. Loktev A, Lindner T, Burger EM, et al. Development of fibroblast activation protein-targeted radiotracers with improved tumor retention. *J Nucl Med.* 2019;60: 1421–1429.
21. Röhrich M, Syed M, Liew DP, et al. ^{68}Ga-FAPI-PET/CT improves diagnostic staging and radiotherapy planning of adenoid cystic carcinomas: imaging analysis and histological validation. *Radiother Oncol.* 2021;160:192–201.
22. Dohi O, Ohtani H, Hatori M, et al. Histogenesis-specific expression of fibroblast activation protein and dipeptidylpeptidase-IV in human bone and soft tissue tumours. *Histopathology.* 2009;55:432–440.